Computation of Three-Dimensional Viscous Linear Cascade Flows

Dochul Choi* and Charles J. Knight†
Avco Research Laboratory, Inc., Everett, Massachusetts

A three-dimensional viscous cascade code has been developed for linear cascades with flat, parallel endwalls. It employs scalar implicit approximate factorization, a finite-volume formulation, second-order upwind differencing, and a two-equation q-ω turbulence model based on integration to the wall. A special form of the thin-layer approximation for the compressible Navier-Stokes equations is used which gives accurate skin-friction predictions on highly skewed meshes, now based on sheared H-grids. This code has been validated by considering three-dimensional viscous flows in Langston's large-scale turbine blade geometry. This validation includes three-dimensional heat-transfer predictions. Agreement with experiment is quite good.

Introduction

IN developing a modern gas-turbine engine, development effort, cost, and time can be reduced substantially through use of analytical design tools and numerical flow models that can predict performance characteristics. The key is generating a computer code that is reliable, efficient, and validated by comparison to high-quality experimental results.

A new computer code has been developed known as HCAS3D. This code solves the "thin-layer" Navier-Stokes equations with a two-equation turbulent model in curvilinear coordinates using a time-asymptotic method for steady-state solutions. It employs sheared H-grids stacked in the spanwise direction, with careful control of near-wall grid spacing to assure sublayer resolution. Preliminary evaluation of this code is discussed in an earlier paper,[1] applying it to the three-dimensional viscous flow for the NASA Energy Efficient Engine vane studied experimentally by Kopper et al.[2] The accuracy of the code was assessed through comparison to experimental data. Particularly, computed loss and flow angle at the exit plane were very promising.

This study describes application of HCAS3D to three-dimensional viscous flows of a large-scale turbine blade cascade case studied experimentally by Langston et al.[3] and a three-dimensional heat-transfer experiment done by Graziani et al.[4] in the same cascade geometry. Comparisons with experiment illustrate the accuracy of the code and its potential use as a viable design tool. Since the formulation and numerical method were explained in our previous paper,[1] only a brief discussion of that is included in this paper. The main focus is comparison of computational results to experiment for code validation.

Numerical Method

A scalar implicit approximate factorization algorithm with a cell-based formulation[1] has been used in the linear cascade code. To maintain high-performance characteristics of the implicit method, boundary conditions are treated fully implicitly. This is essential to achieve a rate of convergence in fine-grid viscous regions comparable to that of the inviscid-core regions. Implicit boundary treatment is particularly important with two-equation turbulence modeling.

Presented as Paper 88-0363 at the AIAA 26th Aerospace Sciences Meeting, Reno, NV, Jan. 11-14, 1988; received Feb. 5, 1988; revision received Aug. 8, 1988.

*Principal Research Scientist. Member AIAA.
†Director, Engine Technology. Member AIAA.

For the explicit procedure (evaluation of residuals), second-order upwinding is used with a cell-based formulation. The numerical dissipation for this scheme is evaluated based on nonconservative variables and characteristic increments given by Roe-averaging[5] at cell faces. For the implicit procedure, first-order upwinding (solving a series of scalar tridiagonal linear systems) is used. This may affect convergence rate somewhat, but the computational cost per time-step is relieved. When accurate steady-state solutions are the only concern, this implicit procedure can be more efficient, in terms of CPU time, than a second-order upwinding procedure.

Two-Equation Turbulence Model

Coakley's q-ω turbulence model[6] has been used due to its numerical compatibility with the asymptotic time-integration method; that is, time-step restrictions due to the turbulence source terms are minimal compared to other two-equation models. The turbulence source terms are treated through a postprocessing step rather than incorporating these into the transverse directional implicit update procedure. Integration to the wall is used with resolution down to about $y_+ = 1$. This model was validated by comparison to known flat-plate results, including wake decay. See Ref. 1 for the details.

Results and Discussions

Two sets of test cases will be presented in this paper. One is for a large-scale turbine blade cascade case studied experimentally by Langston et al.[3] The other is for heat-transfer-coefficient prediction for the experiment done by Graziani et al.[4] Both cases are considered with a laminar-flow assumption as well as with turbulence effects embodied in the two-equation turbulence model. The "laminar" cases are run with an inlet velocity profile appropriate to turbulent flow in order to assure the correct incoming vorticity distribution.

Langston Cascade Case

HCAS3D has been applied to the large-scale Langston cascade. The detailed cascade geometry and experimental configuration can be found in Ref. 3. This was done with the cascade set at an air-inlet angle of 44.7 deg, and the upstream inlet Mach number was 0.1. The Reynolds number based on inlet freestream condition and blade axial chord length is 5.9×10^5.

A total number of $81 \times 42 \times 28$ (NX, NY, and NZ) grid points are used. Figure 1 shows the 81×42 H-grid system for each x-y plane, which is stacked on nonuniformly spaced z gridlines in the spanwise direction. Axial grid distributions are

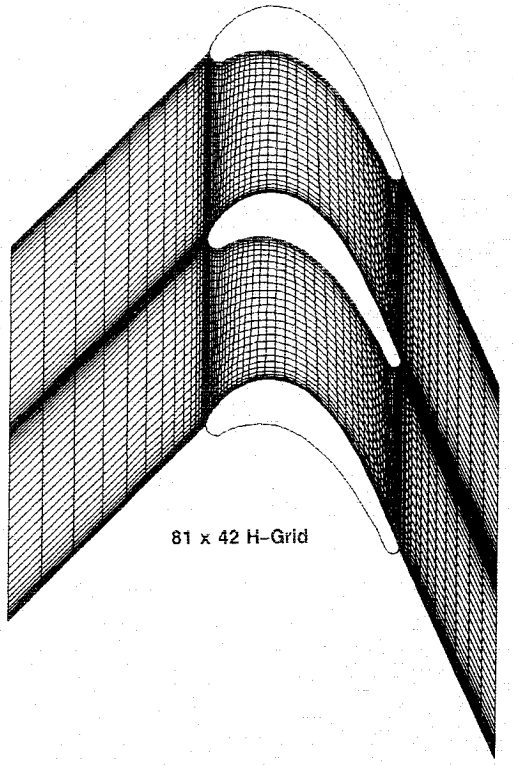

Fig. 1 Algebraically generated grid for Langston cascade case.

chosen to give enough grid points to properly describe the shape of the blunt leading and trailing edges; dy_{min} for the first grid spacing is 10^{-4}, and dy_{max} for the maximum grid spacing is 0.05, both based on axial chord length. In the z direction, dz_{min} is 10^{-4}, and dz_{max} is 0.05 based on chord length. Converged results were achieved with 800 time-steps even with this highly refined grid for good viscous sublayer resolution.

The variation in mass-averaged total pressure loss coefficient C_{pt} is compared with experiment in Fig. 2. Generally, they agree very well. The laminar case shows somewhat lower loss than the turbulent case. Both computations and the experiment show only a small rise in the first half of the blade passage with an increasing rate of loss production toward the trailing edge.

Figure 3 shows the endwall static pressure predictions for the laminar and turbulent cases, and the contours for the q-ω model are compared with experimental results[3] in Fig. 4. Computational results show a local minimum pressure away from the blade in the distribution of pressure coefficients on the endwall. The presence of that minimum and distortion of the static pressure contours upstream are clear evidence of the horseshoe vortex. The limiting streamlines near the endwall (about 0.02% span location) are shown in Fig. 5 for the turbulent case with the experimental plot based on the ink-trace flow visualization. The present predictions show S-shaped limiting streamlines downstream of the primary horseshoe vortex leg, as visualized in the experiment. The predicted saddle point is located slightly upstream of the experimental data. Also, the separation line is somewhat farther displaced from the suction surface at the rear of the blade than in the experiment.

The predicted static pressures at $i=46$ (83% of axial location) are compared to measurements at 82.1% of axial location in Fig. 6. The closed minimum pressure contour near the suction side wall indicates the passage vortex.

Figure 7 shows the development of the predicted mass-averaged total pressure loss at three locations, $i=30$ (14%), $i=39$ (55%), and $i=54$ (96% of axial location) as compared to the experimental data measured at 14%, 55%, and 97% of the

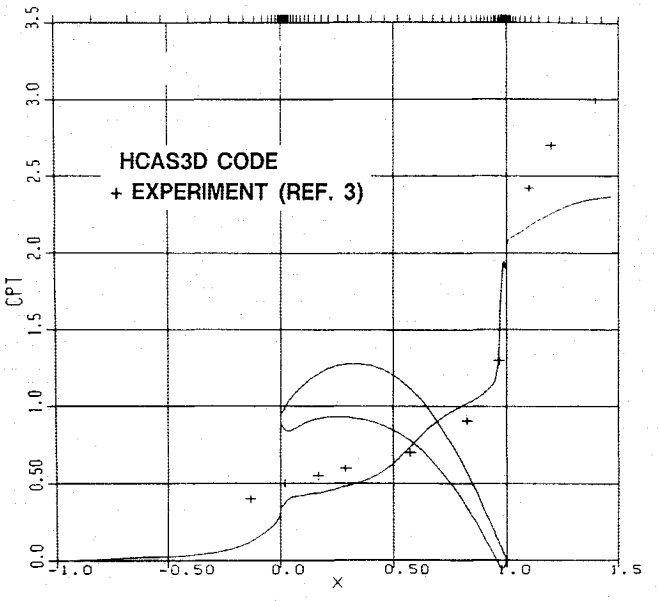

a) Laminar flow

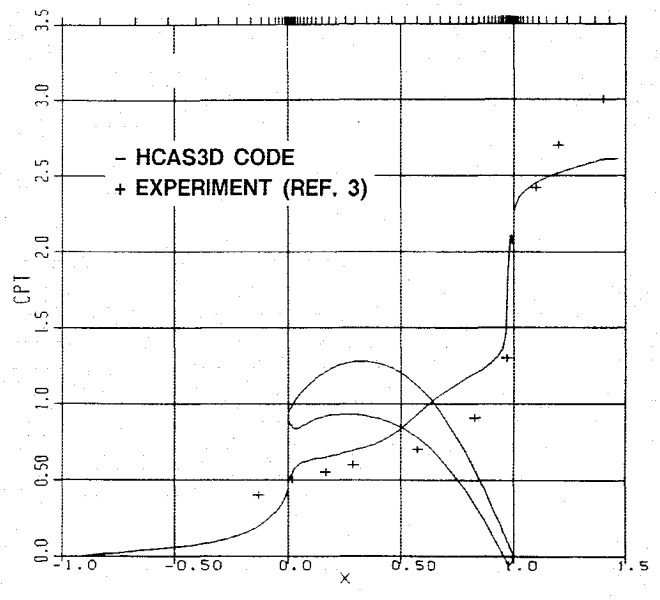

b) q-ω model

Fig. 2 Axial variation of total pressure loss for Langston cascade.

axial location. In this figure, one can clearly recognize the passage-vortex evolution.

Heat-Transfer Prediction

A test case has been executed to validate the code for three-dimensional heat-transfer prediction, comparing to the experiment by Graziani et al.[4] for the Langston cascade. Only the thick inlet boundary-layer case was considered. The basic q-ω model is used without streamline curvature corrections to define baseline performance. Future work should incorporate such efforts as they are known to have significant influence on heat transfer.

Three separate runs were required to produce the information used by the experimentalists to define their "Stanton number,"

$$St = Q_w/\rho_i u_i c_p (T_w - T_{aw}) \quad (1)$$

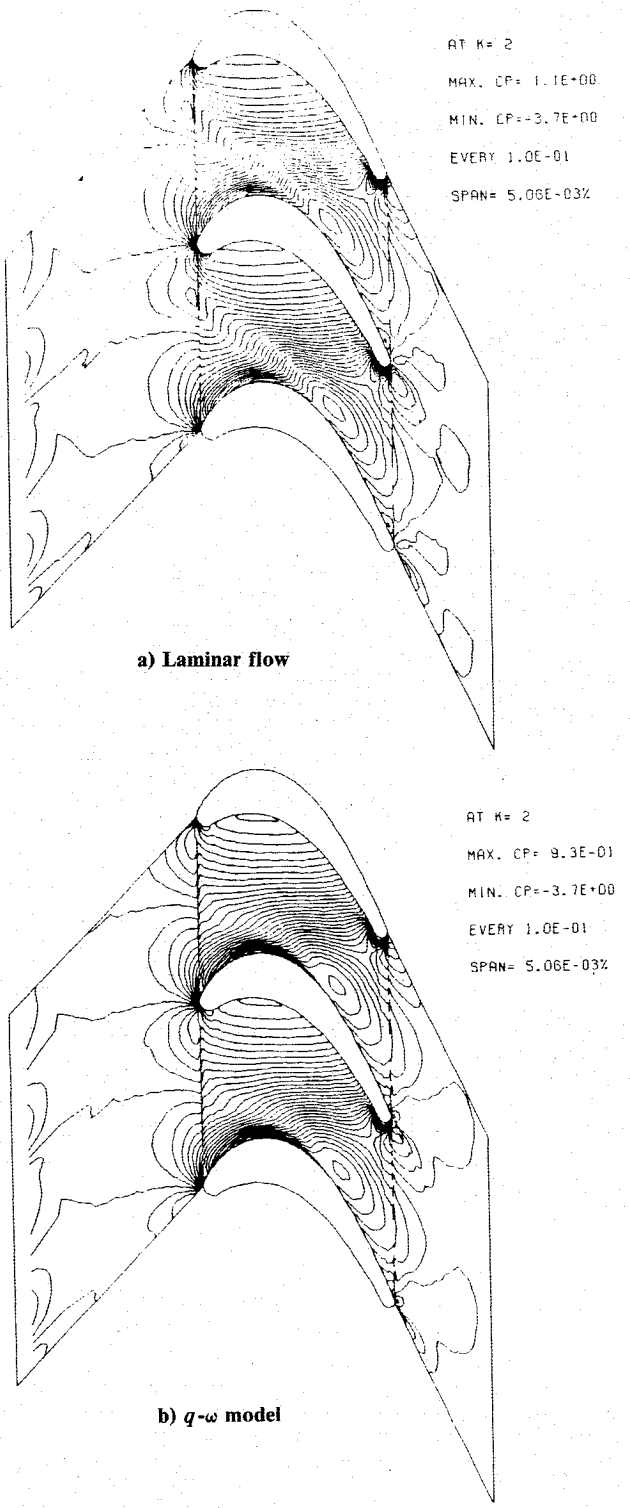

a) Laminar flow

b) q-ω model

Fig. 3 Predicted endwall static pressure coefficient contours.

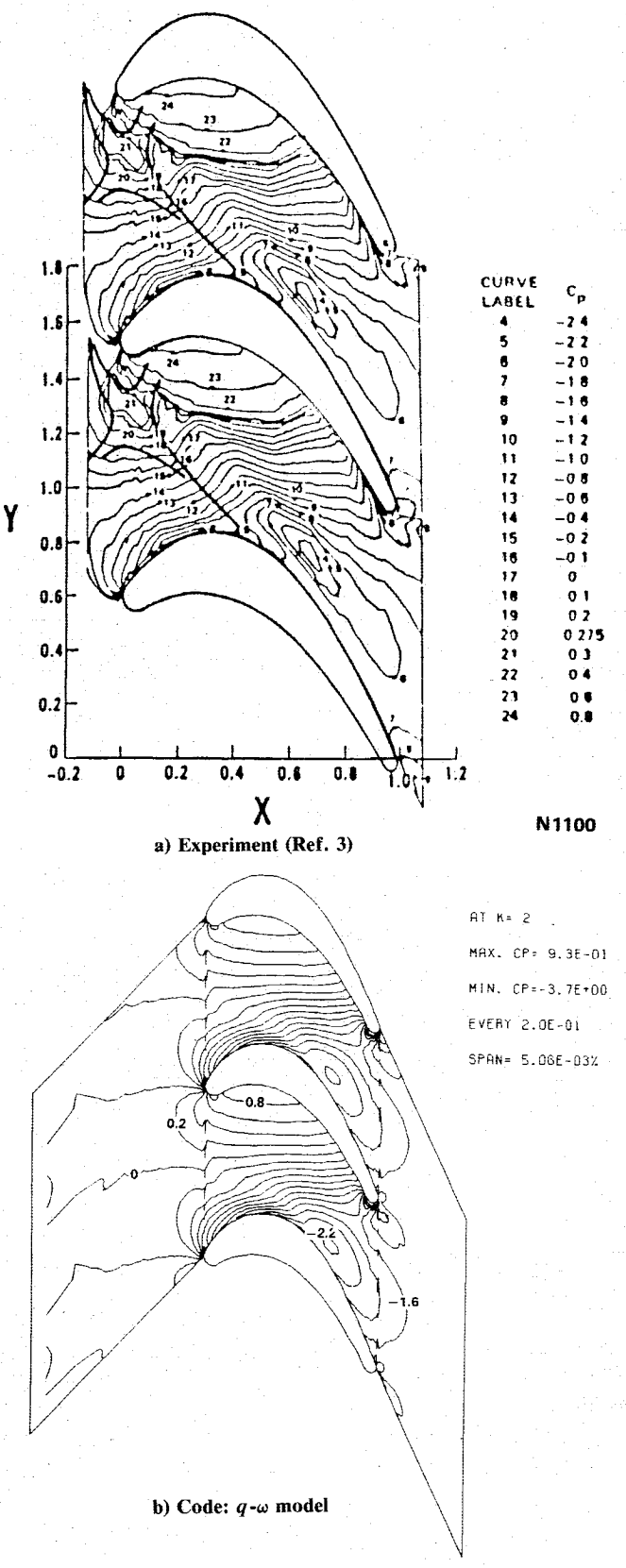

a) Experiment (Ref. 3)

b) Code: q-ω model

Fig. 4 Comparison of measured endwall pressure distribution with predictions based on q-ω model.

where Q_w is the specified heat flux on the airfoil or endwall, subscript i denotes freestream conditions at the inflow plane, c_p is the specific heat at constant pressure, and the two temperatures are to be defined. All runs were made on the same $81\times42\times28$ grid used previously with $DYMN=DZMN=1\times10^{-4}$ and $DYMX=DZMX=0.05$, both based on axial chord length, and each started from the same laminar solution with adiabatic walls via a sudden turn-on of eddy viscosity and altered thermal boundary conditions. Reasonable results were obtained after 600 time-steps, and full convergence was achieved in 800 time-steps. Other parameters are $Pr=0.72$, $Re=6.04\times10^6$ based on stagnation conditions and axial chord length, and $M_e=0.160$, the latter slightly reduced compared to the original Langston experiment.

The first run involved $QFLX1=49.6$ and $QFLX2=69.3$, the normalized heat-flux parameters $Q_w c_x/kT_0$ on the airfoil and endwall, respectively, where Q_w is defined above, c_x is the axial chord, k is the gas thermal conductivity, and T_0 is the stagnation temperature of the incoming flow. The specified values are based on experimental conditions. We were careful to insure that Q_w on the endwall initiated at the same distance

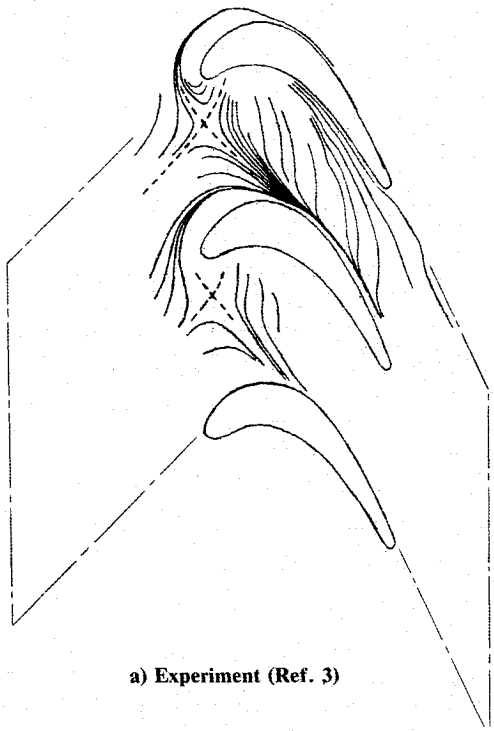

a) Experiment (Ref. 3)

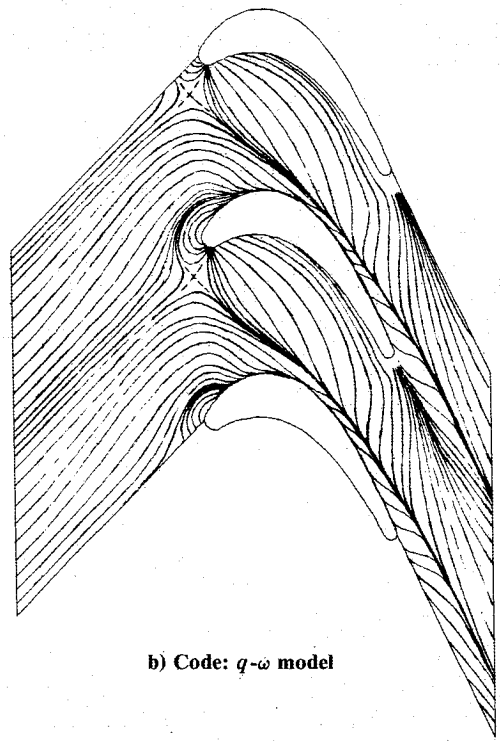

b) Code: q-ω model

Fig. 5 Limiting streamlines on endwall from experiment and HCAS3D code.

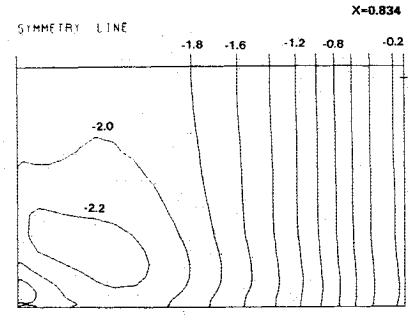

a) Code: laminar flow

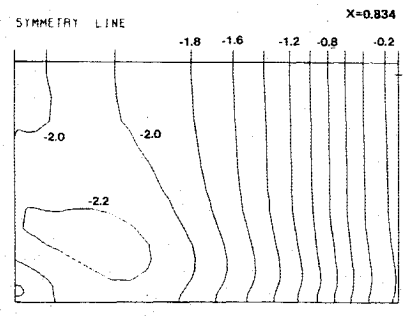

b) Code: q-ω model

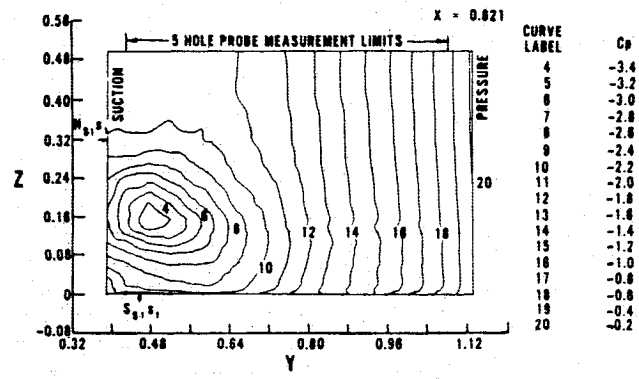

c) Experiment (Ref. 3)

Fig. 6 Static pressure coefficient contours on a selected axial plane.

upstream of the cascade as in the experiment. This run defined the wall temperature T_w entering the Stanton number. The second run involved $QFLX1 = 49.6$ and $QFLX2 = 0$ to determine the adiabatic wall temperature T_{aw} on the endwall, as defined by Graziani et al.[4] Resultant Stanton number contours are shown in Fig. 8. These are in quite reasonable agreement with experiment (i.e., Fig. 8a of Ref. 4). Deviation downstream of the blade is believed to be due to incomplete convergence. This is under further investigation. Note that streamline curvature effects should not be a major factor on the flat endwall.

The third run involved $QFLX1 = 0$ and $QFLX2 = 69.3$ to determine the adiabatic wall temperature T_{aw} on the airfoil surface; T_w was given by the first run as before. Resultant Stanton number contours are shown in Fig. 9, using arc length as the abscissa and the spanwise coordinate as ordinate. Trailing edges are to the left and right on the respective surfaces, and extended lines in the middle indicate the leading-edge line. Agreement with experiment (i.e., Fig. 9a of Ref. 4) is notably poorer, especially in pattern. Part of this is presumbaly due to streamline curvature effects, which suppress turbulence on convex surfaces and enhance it on concave. Another feature apparent in Fig. 9 is that the passage vortex penetrates too far toward midspan on the suction surface as the trailing edge is approached. It is not clear why closely spaced contours start away from the endwall at the leading edge. This may derive from poor resolution near the leading edge with an H-grid, which would mainly affect the suction leg of the horseshoe vortex.

Further information on flow near the airfoil surface is given by the predicted limiting streamlines shown in Fig. 10. Note that there is no clearly defined separation line on the suction surface near the leading edge; instead, it forms well downstream in the computational results. Unfortunately, published experimental results did not include adequate ink traces to make a definitive comparison in that region. The middle of the three streamlines first forming into the separation line is cho-

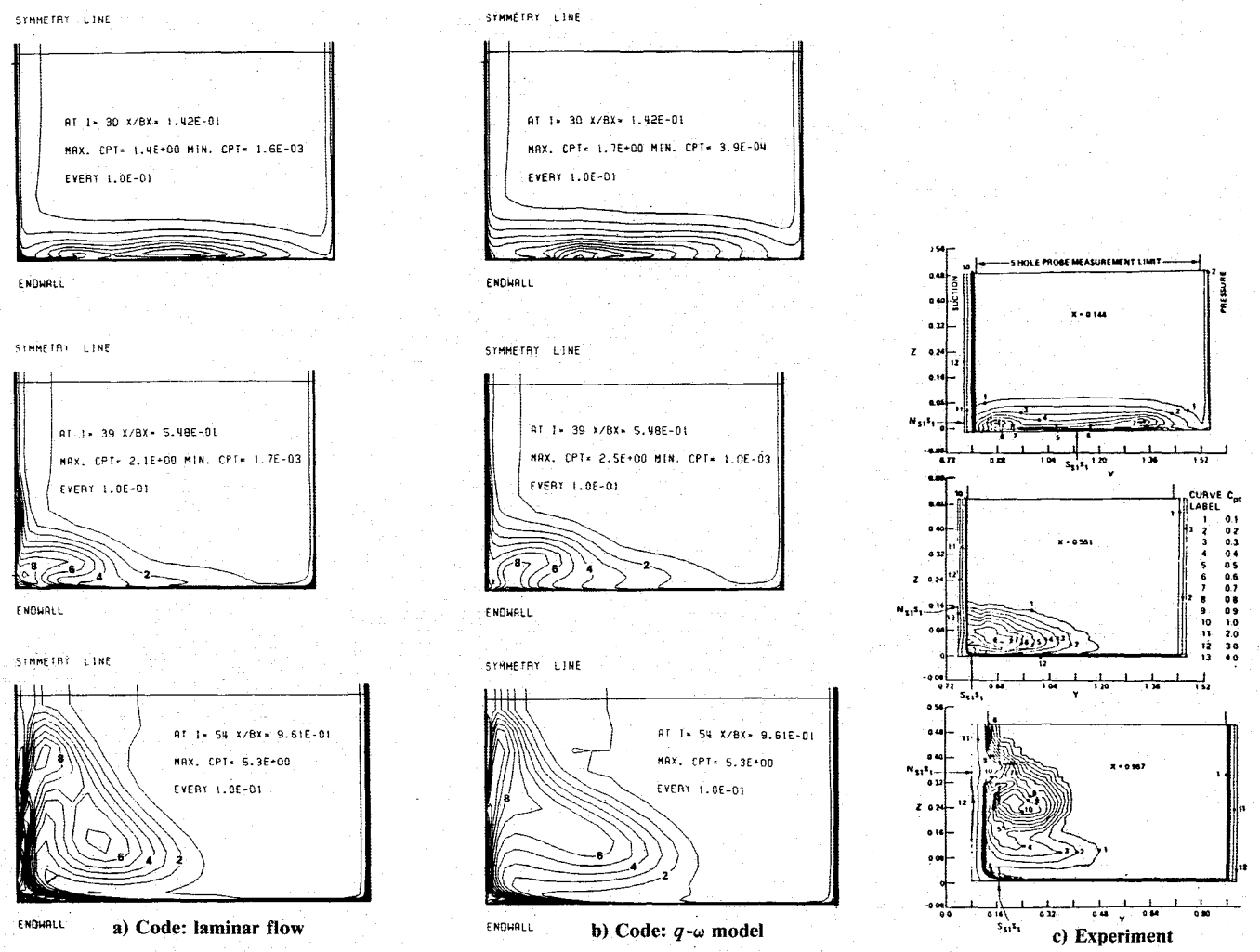

a) Code: laminar flow b) Code: q-ω model c) Experiment

Fig. 7 Total pressure loss coefficient contours on three axial planes.

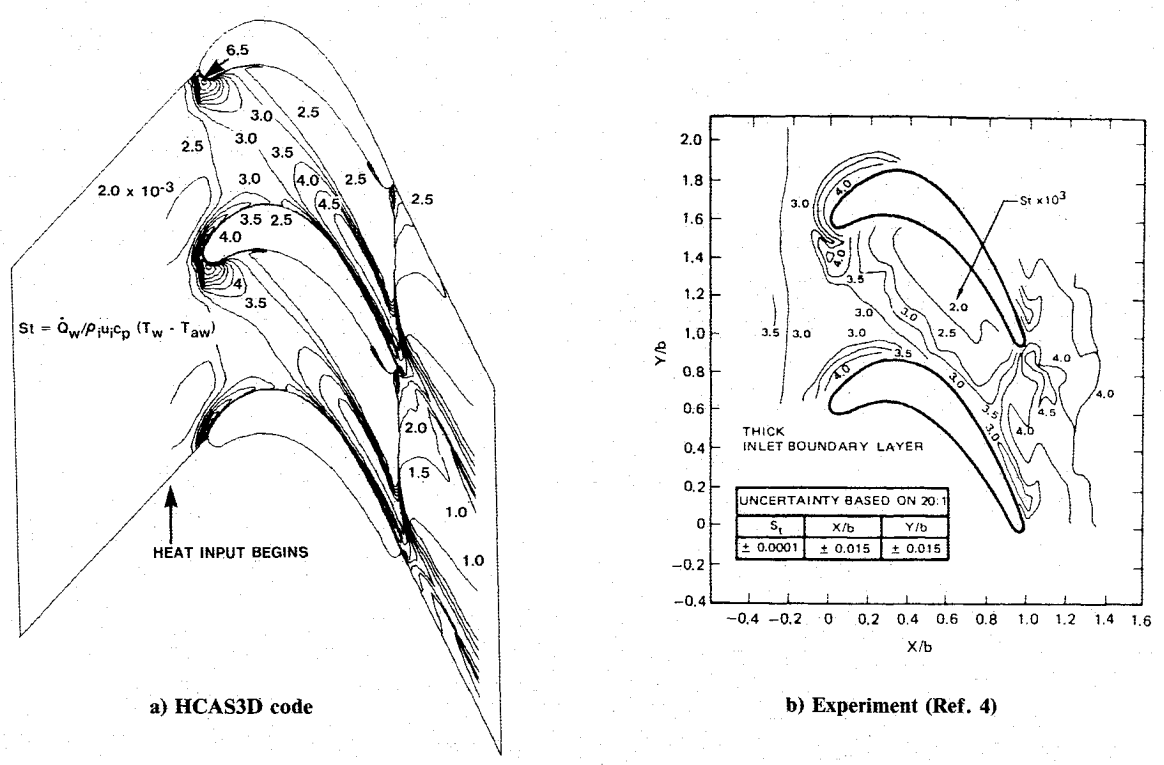

a) HCAS3D code b) Experiment (Ref. 4)

Fig. 8 Endwall Stanton number comparison for Langston cascade.

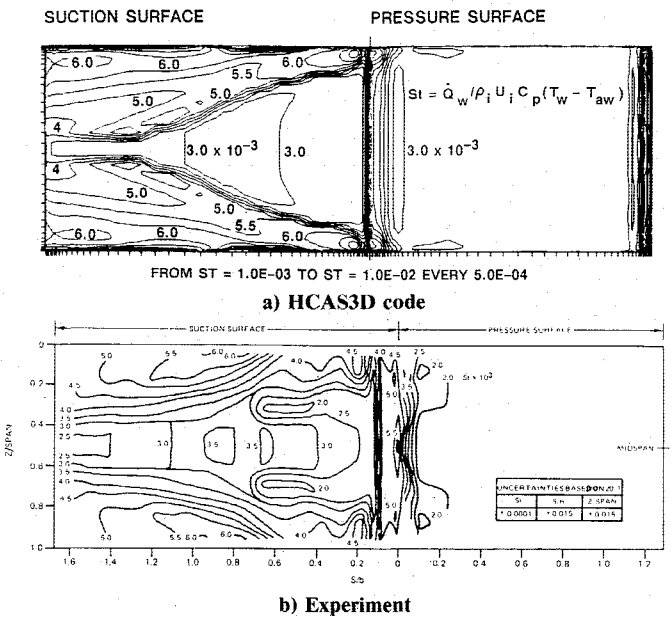

Fig. 9 Stanton number comparison on airfoil surface for Langston cascade, using basic q-ω model.

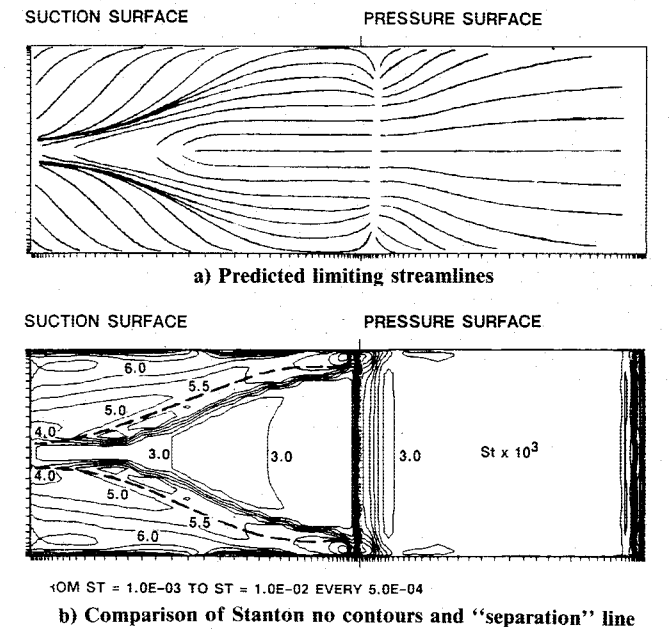

Fig. 10 Predicted phenomenology near airfoil surface of Langston cascade with HCAS3D code.

sen for superposition onto the predicted Stanton contours shown in Fig. 10. From this and the sense of rotation of the two passage vortices, it is evident that closely spaced Stanton contours arise where flow upwells off the suction surface and that higher heat transfer occurs on the other side of the vortices due to freestream gas being engulfed toward the surface. Secondary flow effects on suction surface heat transfer are evidently considerable for this particular cascade.

Conclusion

A newly developed linear cascade code, HCAS3D, has been applied to three-dimensional viscous flows of a large-scale turbine blade cascade case studied experimentally by Langston et al.[3] and a three-dimensional heat-transfer experiment done by Graziani et al.[4] in the same cascade geometry. Computational results on H-grids have been compared to experiment with good agreement. Considering the complexity of the flowfields involved, that is a very significant achievement.

For more accurate heat-transfer prediction, further study on turbulence modeling is appropriate. This study should certainly include streamline curvature correction and influence of inflow freestream turbulence intensity.

Acknowledgment

This research was conducted under the sponsorship of Textron Lycoming's Research and Development Program. The authors wish to thank the Textron Lycoming management for their support and permission to present these results.

References

[1]Knight, C. J. and Choi, D., "Development of a Viscous Cascade Code Based on Scalar Implicit Factorization," AIAA Paper 87-2150, June 1987.

[2]Kopper, F. C. and Milano, R., "EEE Component Development and Integration Program, High-Pressure Turbine Supersonic Cascade Technology Report," NASA CR-165567, Nov. 1981.

[3]Langston, L. S., Nice, M. L., and Hopper, R. M., "Three-Dimensional Flow Within a Turbine Cascade Passage," *ASME Journal of Engineering for Power*, Vol. 99, Jan. 1977, pp. 21-28.

[4]Graziani, R. A., Blair, M. F., Taylor, J. R., and Mayle, R. E., "An Experimental Study of Endwall and Airfoil Surface Heat Transfer in a Large-Scale Turbine Blade Cascade," *ASME Journal of Engineering for Power*, Vol. 102, April 1980, pp. 257-267.

[5]Roe, P. L., "Approximate Riemann Solvers, Parameter Vectors, and Difference Schemes," *Journal of Computational Physics*, Vol. 43, Oct. 1981, pp. 357-372.

[6]Coakley, T. J., "Turbulent Modeling Methods for the Compressible Navier-Stokes Equations," AIAA Paper 83-1693, July 1983.